Journal of Non-Crystalline Solids 502 (2018) 54–61

Contents lists available at ScienceDirect

Journal of Non-Crystalline Solids

journal homepage: www.elsevier.com/locate/jnoncrysol

GeO_2 activated tellurite tungstate glass: A new candidate for solid state lasers and fiber devices

B.C. Jamalaiah

Department of Physics, Rajeev Gandhi Memorial (RGM) College of Engineering and Technology, Nandyal 518501, Andhra Pradesh, India

ARTICLE INFO

Keywords:
Tellurite tungstate glasses
Effect of germanium
Solid state lasers
Optical fiber devices

ABSTRACT

Different amounts of GeO_2 activated tellurite tungstate glasses were prepared by melt quenching technique. Thermal stability and glass forming ability were studied using differential scanning calorimetry. The chemical composition, homogeneity and amorphous nature of studied glasses were investigated. The phonon energy was estimated to be 721.34 cm^{-1}. Experimentally determined refractive indices were compared with those determined from optical band gap (E_g) and optical electronegativity ($\Delta\chi^*$). The dielectric constant (K) and electronic polarizability (α) were determined using refractive index value. The presence of disorder was estimated in terms of Urbach energy (E_U). The average electronegativity (χ_{ave}), oxide ion polarizability ($\alpha_O{}^{2-}$) and covalent character (C_{cov}) were determined. The content of GeO_2 was optimized to be 10.0 mol% to design a novel host material for solid state lasers and fiber devices.

1. Introduction

To meet the requirement of current fast growing technology, new and novel glass hosts with high quantum efficiency have to be designed. Glasses have been extensively used as laser hosts and fiber devices due to their high thermal stability, long chemical durability and good fluorescence properties [1,2]. They find wide range of applications in industry, medical, defense and science & engineering fields. Oxide glasses are of interest in designing laser hosts, fiber amplifiers, dispersion control materials, switches, sensors etc., due to their excellent linear and non-linear optical properties [3–5]. The success of fiber technology in optical communication initiated the researchers to produce new class of glass hosts for variety of applications. In addition, the glasses containing heavy metal oxides such as PbO, Ag_2O, TeO_2, GeO_2, WO_3 and Bi_2O_3 are promising materials for various photonic applications.

Among the available silicate, borate, phosphate glasses, the tellurite glasses are of interest for variety of technological applications due to their distinctive properties such as high refractive index, high dielectric constant, low melting temperature (≤800 °C), low glass transition temperature (≤400 °C), high corrosion resistance, non-hygroscopic and transparency in Vis-NIR regions [6–8]. In case of tellurite based glasses, the TeO_4 trigonal bipyramid (tbp), TeO_{3+1} polyhedra and TeO_3 trigonal pyramid (tp) asymmetric structural units are sensitive to the glass composition and facilitate them to be applicable for variety of photonic devices. A suitable network modifier breaks the Te—O—Te bonds and transforms the Te coordination polyhedron from TeO_4 tbps to TeO_3 tps with the formation of non bridging oxygens (NBO). The doping of small amount of one network former oxide by another glass former oxide enhances both the conductivity and thermal stability [9].

It is well known that tungsten oxide is a good network glass former and its structure is formed by WO_6 and WO_4 groups. When WO_3 is added to TeO_2 based glasses, the WO_4 polyhedra replace a part of TeO_4 tbps and modifies the properties of TeO_2 glasses [10]. The structural and optical properties of binary TeO_2-WO_3 glass systems were investigated for different applications [11–14]. Ternary tellurite glasses such as TeO_2-WO_3-Ag_2O [10], TeO_2-WO_3-Sb_2O_4 [15], TeO_2-WO_3-Ga_2O_3 [15], TeO_2-WO_3-Bi_2O_3 [16], TeO_2-WO_3-PbO [16], TeO_2-WO_3-Ag_2O [17], TeO_2-WO_3-K_2O [18] were prepared and investigated through structure, ionic conduction, thermal stability, heat capacity, magneto-optical studies. Upender et al. [19] studied the structural, physical and thermal properties of WO_3-GeO_2-TeO_2 glasses for rare earth doped fiber devices by varying the WO_3 content. It is well known that GeO_2 influence the chemical resistance and glass transition temperature of amorphous solids [14]. Since GeO_2-based glasses have large range of working temperature ($\Delta T = T_g - T_c$), the addition of GeO_2 enhances the thermal stability and glass forming ability of tellurite glasses [20,21].

The present research work is aimed to select a tellurite tungstate glass containing optimum GeO_2 for trivalent rare earth ions activated solid state lasers, fiber amplifiers, sensors etc., with high quantum efficiency and considerably low non-radiative losses. Thermal, structural and optical properties of TeO_2-WO_3-GeO_2 glasses were studied through differential scanning calorimetry (DSC), powder X-ray diffraction

E-mail address: bcjphysics@gmail.com.

https://doi.org/10.1016/j.jnoncrysol.2018.03.032
Received 21 December 2017; Received in revised form 2 March 2018; Accepted 12 March 2018
Available online 19 March 2018

(XRD), Fourier transform infrared (FTIR), scanning electron microscope-energy dispersive X-ray spectrum (SEM-EDS) and optical absorption spectra. The effect of GeO_2 on different optical properties such as refractive index (n), optical band gap energy (E_g), electronegativity (χ), oxide ion polarizability ($\alpha_{O^{2-}}$) and optical basicity (Λ) was discussed.

2. Experimental

2.1. Materials and method of preparation

Different amounts of GeO_2-doped tellurite tungstate glasses of composition (95-x) TeO_2-5 WO_3-x GeO_2, where $x = 0$, 1.0, 5.0, 10.0 and 20.0 mol%, were prepared by conventional melt quenching technique. About 20 g batches of homogeneous powders were prepared using high purity TeO_2 (Aldrich, ≥99%), WO_3 (Aldrich, ≥99%) and GeO_2 (Aldrich, ≥99.99%). These powders were heat treated at 875 °C for 40 min in alumina crucibles using a programmable electric furnace. The melt was air-quenched on a pre-heated brass plate and annealed at 300 °C for 10 h to remove the thermal strains occurred during quenching process. For convenience, the prepared glass samples were referred as TWG0, TWG1, TWG5, TWG10 and TWG20 glasses for $x = 0$, 1.0, 5.0, 10.0 and 20.0 mol%, respectively.

2.2. Physical and optical characterization

The glass samples were polished for optical quality with a thickness of about 0.15 ± 0.01 cm. Different physical, electrical and optical properties of TWGx glasses are summarized in Table 1. The measurements of density (ρ) are essential to describe the tightness and changes in structure of materials. The Archimedean principle was applied to find the densities of TWGx ($0 \le x \le 20.0$ mol%) glasses with distilled water as immersion liquid.

$$\rho = \frac{W_1}{(W_1 - W_2)} \times \rho_w \quad (1)$$

where W_1 is the weight of sample in air, W_2 is the weight of sample in water and ρ_w is the density of water (1.0 g/cm^3). The density of TWGx glasses (see Table 1) decrease with increase of GeO_2 content as illustrated in Fig. 1. Similar results were reported for germanotellurite glasses [22]. The refractive indices were determined with Abbes refractometer (Model No. R-4, Advanced Research Instruments Company, New Delhi) using 1-bromonaphthalene as an adhesive fluid and sodium vapour lamp ($\lambda = 589.3$ nm) as a light source. The values of refractive index decrease with increase of GeO_2 content. The variation of refractive index as a function of GeO_2 is also shown in Fig. 1.

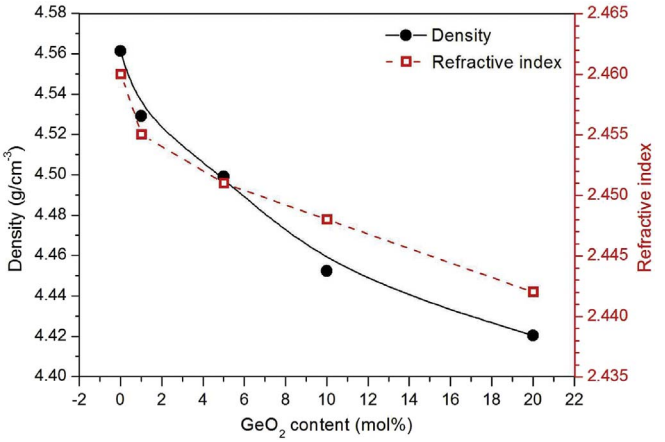

Fig. 1. Variation of density and refractive index as a function of GeO_2 content in TWGx glasses.

The refractive indices were used to determine the dielectric constant, K ($=n^2$) and also the reflection losses, $R = [(n-1)^2/(n+1)^2]$. For TWGx glasses, the reflection losses are found to be nearly 18%. These results indicate that most of the energy of incident light has been either absorbed or transmitted by the TWGx glasses. The refractive index was also used to estimate the molar refractivity (R_M) which is a measure of polarizability of materials.

$$R_M = \left(\frac{n^2 - 1}{n^2 + 2}\right) \times V_M \quad (2)$$

where $V_M = (\overline{M_i}/\rho)$ represents the molar volume which is a measure of structure compactness of materials and it depends on density and total molecular weight of the material. The factor $\overline{M_i}(=x_i \times Z_i)$ represents the average molecular weight of the glass system. Here x_i and Z_i represents

Table 1
Sample thickness (l), density (ρ), refractive index (n), dielectric constant (K), reflection losses (R), average molecular weight ($\overline{M}$), molar volume (V_M), molar refractivity (R_M), metallization criterion (M), polarizability constant (α), optical basicity (Λ), optical band gap energy (E_g), band tailing parameter (B), Urbach energy (E_U), average electronegativity (χ_{ave}), oxide ion polarizability ($\alpha_O{}^{2-}$), glass electronegativity (χ_{glass}) and covalent character (C_{cov}) for TWGx glasses.

Parameter	TWG0	TWG1	TWG5	TWG10	TWG20
l ± 0.01 cm	0.15	0.15	0.15	0.15	0.15
ρ ± 0.01 g/cm^3	4.56	4.53	4.50	4.45	4.42
n ± 0.001	2.460	2.455	2.451	2.448	2.442
n (E_g)	2.442	2.439	2.433	2.430	2.424
n ($\Delta\chi^*$)	2.553	2.549	2.542	2.539	2.532
K ± 0.02	6.05	6.03	6.01	5.99	5.96
R ± 0.02%	17.81	17.73	17.68	17.64	17.55
$\overline{M}$ ± 0.01 g	163.21	163.16	162.94	162.66	162.11
V_M ± 0.02 cm^3	35.78	36.02	36.21	36.53	36.67
R_M ± 0.02 cm^3	22.45	22.56	22.65	22.82	22.86
M ± 0.001	0.373	0.374	0.375	0.376	0.377
α ± 0.02 × 10^{-24} cm^3/mol	8.90	8.95	8.98	9.05	9.07
Λ_{Th} ± 0.001	0.964	~0.964	0.963	0.962	0.960
Λ_{χ} ± 0.001	0.905	0.905	0.906	0.906	0.907
$\Lambda_{\alpha_o{}^{2-}}$ ± 0.001	0.959	0.959	0.960	0.960	0.961
E_g ± 0.02 eV	2.84	2.85	2.87	2.88	2.90
B ± 0.02	1.80	2.00	2.25	2.57	3.00
E_U ± 0.04 eV	1.48	1.56	2.99	3.17	3.96
χ_{ave} ± 0.002	3.005	3.004	3.003	3.002	2.999
$\alpha_O{}^{2-}$ ± 0.002 × 10^{-24} cm^3/mol	2.348	2.350	2.351	2.352	2.354
χ_{glass} ± 0.003	1.327	1.328	1.332	1.336	1.345
C_{cov} ± 0.03%	71.77	71.75	71.69	71.60	71.44

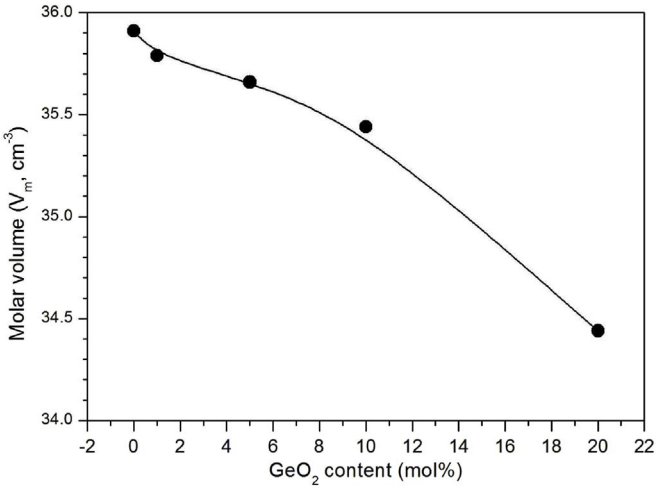

Fig. 2. Variation of molar volume as a function of GeO_2 content in TWG*x* glasses.

the mole fraction and molar weight of constituent oxides, respectively. The addition of GeO_2 causes a decrease in molar volume of TWG*x* glasses. The variation of molar volume as a function of GeO_2 is presented in Fig. 2. The values of R_M have been used to determine the polarizability constant (α) of a glass using the following formula.

$$\alpha = \left(\frac{3}{4\pi N_A}\right)\cdot R_M \tag{3}$$

where N_A ($=6.022 \times 10^{23}\,mol^{-1}$) called the Avogadro constant. From Table 1 one can notice that the polarizability of TWG*x* glasses increase with increase of GeO_2 content.

To investigate the thermal stability, glass forming ability and amorphous nature, the TWG*x* glass samples were crushed well and grinded into a fine powder of particle size of nearly 60 μm. The crystallization process was examined by DSC thermograms obtained with a Labsys™ TG-DSC-16 thermal analyzer under air atmosphere at a heating rate of 15 °C/min. The amorphous nature of TWG*x* glasses was confirmed by XRD profiles obtained on X'Pert-Pro Materials Research Diffractometer ($\lambda_{CuK\alpha}$ = 1.5406 Å). The FTIR absorption spectra were recorded with a Thermo Nicolet IR200 FTIR spectrophotometer by KBr pellet method. The SEM-EDS analysis was carried out on Hitachi SU-70 scanning electron microscope attached to Bruker Nano GmbH Berlin setup and X-Flash 4010 detector. The optical absorption measurements were carried out on Perkin Elmer Lambda 950 spectrophotometer.

3. Results

3.1. Thermal analysis

Glass transition temperature (T_g), crystallization temperature (T_c) and melting temperature (T_m) of prepared glass samples were determined from DSC thermograms illustrated in Fig. 3. The DSC thermograms show a considerable change in T_g and T_c with increase of GeO_2 content. For GeO_2 free glass, the value of T_g is about 377 °C and it changes from 380 to 386 °C when the content of GeO_2 varies from 1.0 to 20.0 mol%. The glass transition is followed by onset crystallization (T_{os}), bulk crystallization (T_c) and glass melting (T_m) temperatures. All these values are obtained with an accuracy of about ± 2 °C and presented in Table 2.

3.2. XRD and FTIR studies

The powder XRD profiles shown in Fig. 4 reveal the glassy/amorphous nature of TWG*x* glasses. It is well known that the IR absorption bands are the characteristics of various vibrational modes of glass

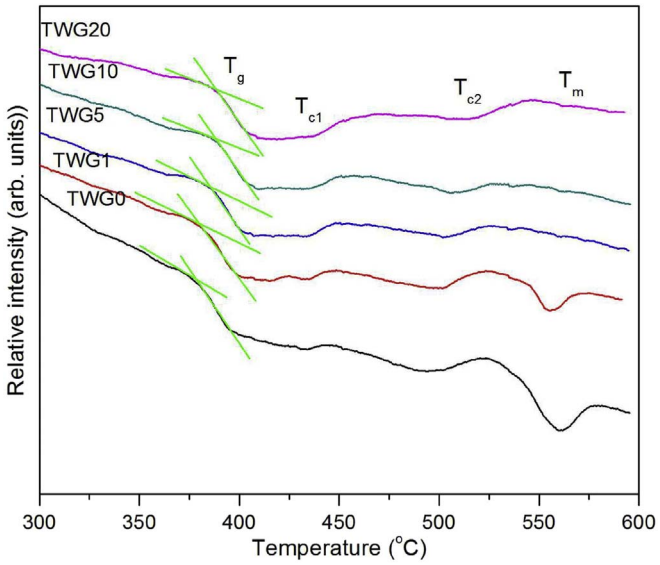

Fig. 3. DSC thermograms of TWG*x* glasses.

Table 2
Glass transition temperature (T_g), on set crystallization temperature (T_{os}), crystallization temperature (T_c), thermal stability (ΔT) and Herby number (H_R) for TWG*x* glasses.

Glass	T_g (°C)	Crystalline temperature		T_m (°C)	ΔT (°C)	H_R
		T_{os} (°C)	T_c (°C)			
TWG0	377	430	495	540	118	2.62
TWG1	380	434	501	545	121	2.75
TWG5	382	435	504	549	122	2.71
TWG10	385	437	511	560	126	2.57
TWG20	386	439	518	563	132	2.93

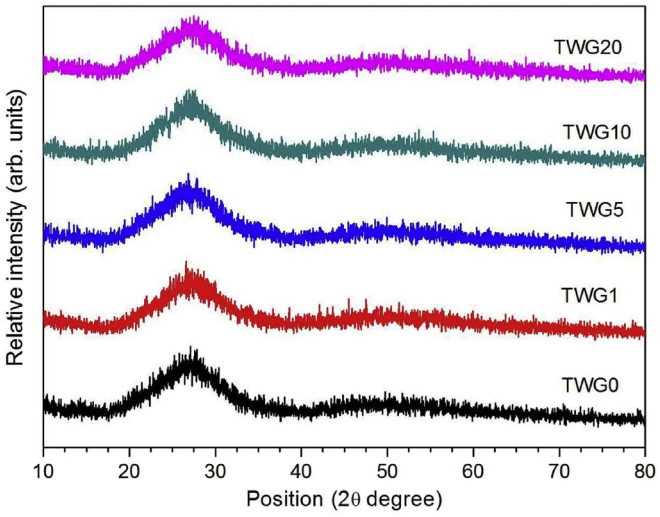

Fig. 4. Powder XRD profiles of TWG*x* glasses.

network and metallic cations. However, no two unique molecules produce the same IR spectra. When IR radiation is allowed to passes through a sample then a part of incident radiation is absorbed by the sample and the rest is transmitted through the sample. The FTIR spectra shown in Fig. 5 give the information regarding the presence of various bonds responsible for the formation of TWG glass matrix.

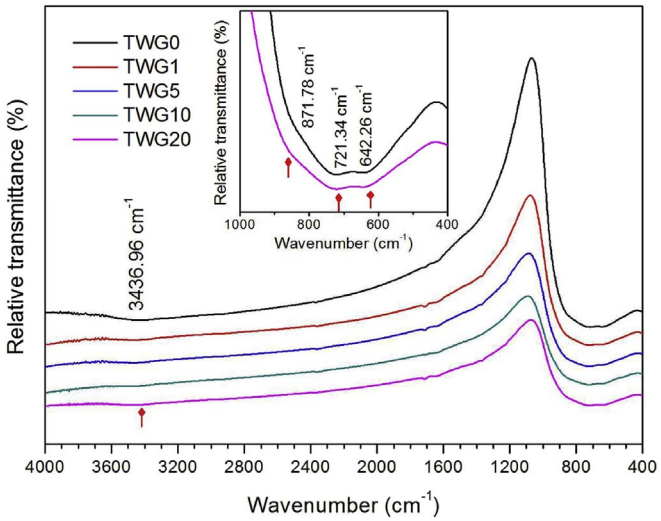

Fig. 5. FTIR spectral profiles of TWG*x* glasses.

3.3. Absorption spectra

It is well known that to understand the band structure and energy gap of both crystalline and amorphous materials, the optical absorption analysis is one of the useful methods. Further, the investigation of optically induced electronic transitions requires the optical absorption coefficient near the fundamental absorption edge. To measure the absorption coefficient, the room temperature optical absorption spectra of TWG*x* glasses were recorded in the visible spectral region and shown in Fig. 6(a). These spectra reveal that the absorption edges are not sharply defined for the studied glasses supporting the amorphous nature identified by the XRD studies. However, the absorption edge is found shifted towards the shorter wave length region with increase of GeO_2 content. The same was also confirmed from the optical transmission spectra shown in Fig. 6(b). The shift in absorption edge towards the shorter wavelength region is an indication of decrease of number of non bridging oxygen's (NBOs) with increase of GeO_2 in TWG*x* glass matrix [23].

4. Discussion

4.1. Thermal stability and glass forming ability

The DSC thermogram of any material exhibits an endothermic peak due to glass transition temperature (T_g) and an exothermic peak (T_c) due to the crystal growth followed by another endothermic peak at relatively high temperature, called melting temperature (T_m) due to the melting effect. In order to fabricate a fiber or a laser host, the glasses should have high thermal stability ($\Delta T = T_c - T_g$) and low temperature interval (T_m–T_c). Monteiro et al. [22] reported that the addition of GeO_2 to a tellurite glass enhances the fiber drawing ability. In the present case the on-set crystallization temperature (T_{os}) varies from 380 to 386 °C and the crystallization temperature (T_c) changes from 501 to 518 °C when the GeO_2 content varies from 1.0–20.0 mol%, while the value of T_m varies from 545 to 563 °C. The values of (T_m–T_c) are found to be 40, 44, 45, 49 and 45 for x = 0, 1.0, 5.0, 10.0 and 20.0 mol%, respectively. From the literature [24] it is clear that the glass transition temperature depends on the density of covalent cross-linking, the oxygen density of the network and the number and strength of cross-links between oxygen and cation. In the present research work, the addition of GeO_2 causes an increase in T_g. This could be due to decreased number of NBOs. The DSC thermogram is also important for a qualitative estimation of ΔT and the Herby number (H_R) which is a measure of the tendency of a composition to become a glass rather than crystal [25].

$$H_R = \left(\frac{T_c - T_g}{T_m - T_c}\right) \tag{4}$$

Higher the values of ΔT and H_R larger will be the thermal stability and glass forming ability, respectively. Considerably higher values of H_R and ΔT show an excellent glass forming ability and high thermal stability of TWG*x* glasses, respectively. The values of ΔT increase with increase of GeO_2 content (see Table 2) due to decreased number of NBOs and viscosity [22]. The values of H_R are found higher than 1T7G [22] and TZNLEu [26] glasses. The values of ΔT are very close to those reported for Nb_2O_5-TeO_2 glasses [27] and GeO_2- and Nb_2O_5-modified tellurite glasses [28].

4.2. SEM-EDS analysis

To investigate the homogeneity, existence of any cluster and the elemental analysis, the SEM-EDS study was carried out for TWG10 glass sample. The SEM image shown in inset of Fig. 7 indicates that the studied glasses are free from clusters and defects. The EDS spectrum shown in Fig. 7 reveals the absence of foreign elements and no change in the chemical composition of TWG*x* glasses. The atomic weight percentage of the elements is also listed in Fig. 7.

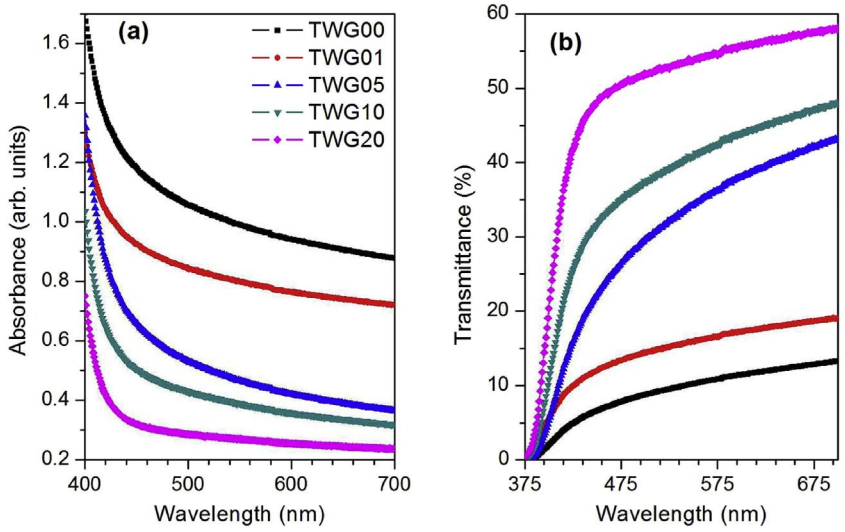

Fig. 6. Optical absorption spectra (a) and transmittance spectra (b) of TWG*x* glasses.

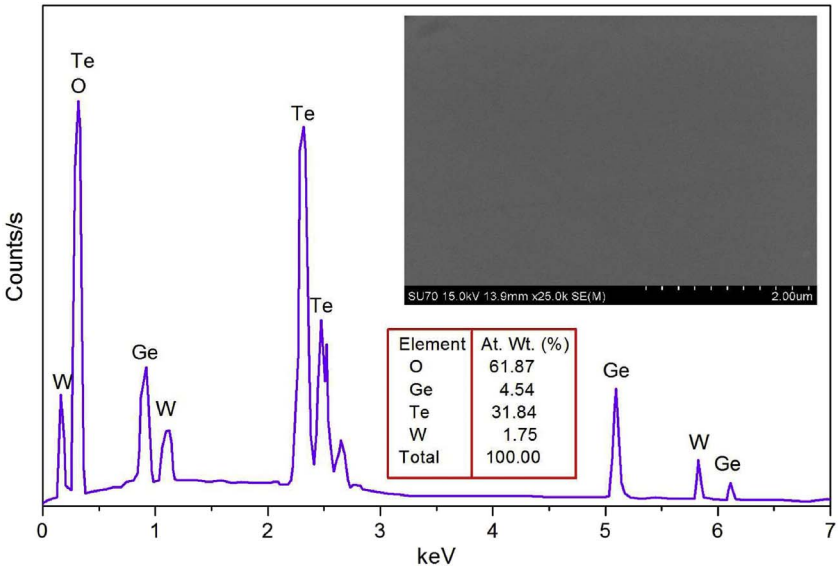

Fig. 7. The EDS spectrum and SEM image (inset) of TWG10 glass.

4.3. Structural analysis

The TWG*x* glass samples are found transparent and free from visible inhomogeneities like bubbles, cracks and inclusions. The XRD profiles shown in Fig. 4 contain (i) no sharp diffraction lines and (ii) a large bump distributed in a wide 2θ range from ~18° to 35° due to multiple scatterings at randomly distributed atoms. The visual transparency, inhomogeneity, absence of sharp diffraction lines and the presence of large bump support that the TWG*x* glasses are pure amorphous in nature.

From the FTIR spectra described in Fig. 5 one can notice no considerable change in the positions of IR absorption bands and an abrupt change in transmittance from 100% to ~80% and then to ~40% when the content of GeO_2 changes from 1.0 mol% to 20.0 mol%. The FTIR spectra of TWG*x* glasses are identical to $(TeO_2)_{100-x}$-$(WO3)_x$, and $(TeO)_{100-x}$-$(ZnC1_2)_x$ glasses [29]. In general, a pure tellurite glass shows an IR absorption band at 640 cm^{-1} owing to three dimensional network composed of TeO_4 tbps units. The TWG*x* glasses exhibit four IR absorption bands at about 642.26, 721.34, 871.78 and 3436.96 cm^{-1} and they are assigned to various vibrational bands [30–32]. The assignment of IR absorption bands is described in Table 3. A relatively weak water band at around 3436.96 cm^{-1} and the absence of OH^- stretching band show that the non-radiative losses are insignificant in TWG*x* glasses. The FTIR spectra confirm the transformation of deformed TeO_4 units into symmetric TeO_3 units. The transmission bands observed below 1000 cm^{-1} are found to have very low intensity leading high absorption in this region. These results indicate that the glass absorption increases with increase of GeO_2 content in the spectral region below 1000 cm^{-1}. Additionally, the highest energy corresponding to the 721.34 cm^{-1} could be treated as phonon energy of TWG*x* glasses, which is in the order of phonon energy of other tellurite based glasses [26,33].

Table 3
Assignment of IR absorption bands of TWG*x* glasses.

IR band position (cm^{-1})	Assignment
3436.96	Fundamental vibrations of H_2O
871.78	Stretching vibrations of Ge—O in GeO_4 and W—O in WO_4 groups
721.34	Stretching vibrations of Te—O in symmetric TeO_3 group
642.26	Stretching vibrations of Te—O in deformed TeO_4 group

4.4. Optical band gap energy and metallization

The optical band gap energy (E_g) is used to characterize the optical properties of amorphous materials and it can be obtained from the UV–vis absorption spectra. The absorption coefficient,$\alpha(=A/l)$ near the absorption edge of each spectrum (shown in Fig. 6(a)) has been obtained using the absorbance (A) and sample thickness (l). Mott and Davis [34] proposed a relation between α and the photon energy ($h\nu$) of incident radiation for amorphous materials and it is given by

$$\alpha \cdot h\nu = B(h\nu - E_g)^r \quad (5)$$

where B is a constant and it is called band tailing parameter. The parameter r can have values 2, 3, 1/2 and 1/3 corresponding to indirect allowed, indirect forbidden, direct allowed and direct forbidden transitions, respectively. A graph drawn taking the quantity $h\nu$ on X-axis and $(\alpha \cdot h\nu)^{1/2}$on Y-axis is called the Tauc plot. The value of E_g can be obtained from the linear region of Tauc plot, which can be extrapolated to meet $h\nu$ axis at $(\alpha \cdot h\nu)^{1/2} = 0$ [35]. As a reference, the Tauc plots for TWG0 and TWG20 glasses are presented in Fig. 8. The values of E_g

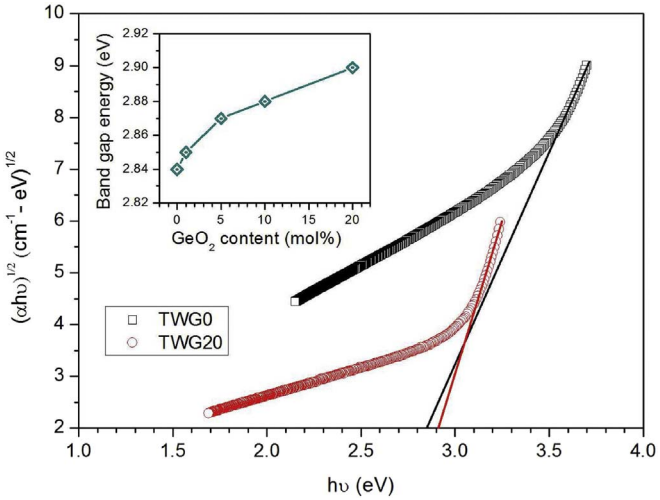

Fig. 8. Tauc plots for TWG0 and TWG20 glasses. Inset shows the variation of band gap as a function of GeO_2 content.

increase with increase of GeO_2 content owing to decreased number of NBOs. It is well known that the electronic levels related to NBOs exist around the top of the valence band. The shift in fundamental absorption edge and the FTIR results show that the number of NBOs decreases with the addition of GeO_2 content. Thus, these results support the estimated values of E_g. The variation of E_g as a function of GeO_2 content is illustrated in inset of Fig. 8. The values of B determined from the slope of Tauc plots increase with increase of GeO_2 content up to 5.0 mol%, reached to a minimum at 10.0 mol% and then increase for further raise of GeO_2 (see Table 1). The values of E_g obtained for TWG*x* glasses are found higher than other tellurite based glasses such as TeO_2-WO_3-ZnF_2 (2.66–2.69 eV) [36], GT1 (2.26 eV) [37], GT2 (2.44 eV) [37] glasses.

The ratio of molar refractivity to molar volume (R_M/V_M) is one of the important parameters used to predict the metallic or non-metallic nature of solids. According to theory of metallization of condensed matter, $(R_M/V_M) > 1$ for metals and $(R_M/V_M) < 1$ for non-metals [38]. The metallization criterion (M) of an amorphous material has been determined using the following equation.

$$M = 1 - \left(\frac{R_M}{V_M}\right) \tag{6}$$

For most of the tellurite glasses, M lies in the range 0.38–0.45 [39]. Moreover, smaller value of M is an indication of increasing the width of valance and conduction bands resulting narrow energy gap. The enhancement of magnitude of M shows an increase in optical band gap energy. In the present investigation, the values of M are found to be in the above said range (see Table 1). The increased values of optical band gaps with increase of GeO_2 content support the metallization criteria.

4.5. Urbach energy

In case of low crystalline or amorphous materials the localized states extend in the forbidden energy gap resulting a band tailing called the Urbach tail. The extent of Urbach tail is the measure of disorder i.e., the number of defects or the lack of crystalline long range order present in the given material. The Urbach tail is an exponential part along the absorption coefficient curve near the optical band edge. The energy corresponding to the Urbach tail is called Urbach energy (E_U) and it can be estimated using the following relation [40].

$$\alpha(\nu) = \alpha_0 \cdot \exp\left(\frac{h\nu}{E_U}\right) \tag{7}$$

where α_0 is a constant. The reciprocal of the slope of 'ln $\alpha(\nu)$ versus $h\nu$' plot gives the magnitude of E_U. Smaller the value of E_U more will be the homogeneity and stability of glass (or) higher the value of E_U more will be the defects and less is the stability of glass. The 'ln $\alpha(\nu)$ versus $h\nu$' plots for TWG*x* glasses are shown in Fig. 9. In the present investigation, the value of E_U increases with increase of GeO_2 content (see Table 1). From the observed values of E_U one can notice that the TWG10 and TWG20 glasses have high homogeneity and stability. The E_U values show a trend similar to band tailing parameters determined from $(\alpha \cdot h\nu)^{1/2}$ vs. $h\nu$ plots. The value of E_U (3.17 eV) obtained for TWG10 glass is found higher than PAAm-GO composites (2.89–2.96 eV) [41].

4.6. Oxide ion polarizability and covalent character

The electronic polarizability is one of the important properties of materials and it is closely related to their applicability in the field of optics and electronics. Dimitrov and Sakka [42] reported that Ge^{4+} ions have higher polarizability compared to P^{5+}, Si^{4+} and B^{3+} ions owing to their small cation unit field strength. Since the Te^{4+} ion possesses single pair electrons in their valance shell, they are said to be highly polarizable. The W^{6+} ions are also highly polarizable due to their empty d-orbitals and high coordination number. Thus, tellurite glasses containing WO_3 and GeO_2 show high oxide ion polarizability. Though,

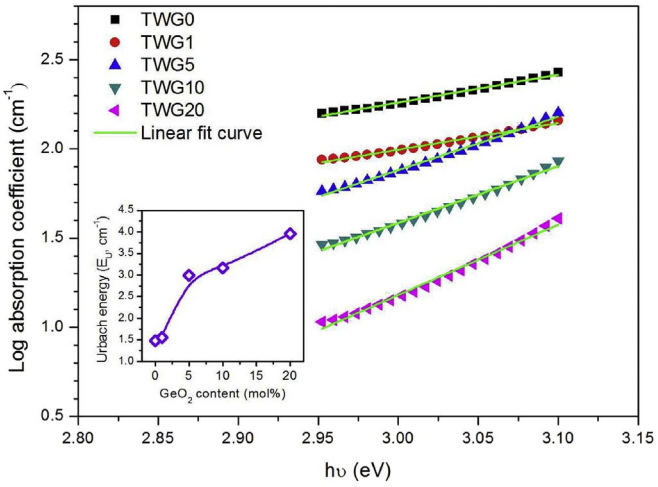

Fig. 9. The ln $\alpha(\nu)$ vs. $h\nu$ plots for TWG*x* glasses. Inset shows the variation of Urbach energy as a function of GeO_2 content.

there exist different formulae, the following empirical relation proposed by R.R. Reddy et al. [43] has been used to determine the oxide ion polarizability ($\alpha_O{}^{2-}$).

$$\alpha_O^{2-} = 4.624 - 0.7569\chi_{ave} \tag{8}$$

where χ_{ave} represents the average electronegativity and it can be obtained using the following relation [44].

$$\chi_{ave} = \frac{\sum_{i=1}^{n} \chi_i \cdot N_i}{\sum_{i=1}^{n} N_i} \tag{9}$$

where χ_i is called the Pauling electronegativity and N_i is the number of atoms of a particular species having electronegativity χ_i. The observed values of χ_{ave} and $\alpha_O{}^{2-}$ (see Table 1) indicate that there is a decreasing tendency for χ_{ave} and increasing tendency for $\alpha_O{}^{2-}$ with the addition of GeO_2 content in TWG*x* glasses. The value of χ_{ave} (3.002 ± 0.002) obtained for TWG10 glass is comparable to 90 TeO_2-10 WO_3 (3.002) [43] and B_2O_3-Li_2O-CuO (3.00) [45] glasses, while the value of $\alpha_O{}^{2-}$ (2.352 ± 0.002 × 10^{-24} cm^3/mol) is comparable to 90 TeO_2-10 WO_3 (2.292 × 10^{-24} cm^3/mol) [43] and TeO_2-WO_3 (2.344 × 10^{-24} cm^3/mol) [5] glasses.

Further, the difference of average electronegativity of anions (χ_A) and cations (χ_C) is called the electronegativity of a glass (χ_{glass}) composition and it can be used to estimate the degree of covalent bonding character (C_{cov}) of that glass. According to Pauling [46] the relation between C_{cov} and χ_{glass} is given by

$$C_{cov} = \exp\ (-0.25\chi_{glass}^2) \tag{10}$$

where $\chi_{glass}(=\chi_A - \chi_C)$. According to Eq. (10), the value of C_{cov} decrease exponentially with increase of χ_{glass}. In the present investigation, the values of χ_{glass} are found increase while the values of C_{cov} decrease with the addition of GeO_2 content (see Table 1). The experimental results indicate that the covalent character of TWG*x* glasses is of the order of ~72% which is comparable to LBTAFNd glass [47].

4.7. Optical basicity

Optical basicity (Λ) is particularly useful for crystalline and vitreous oxide network systems to know the average electron donor power of all the oxide (II) atoms present in the medium. The theoretical optical basicity (Λ_{Th}) for TWG*x* glasses can be obtained using the relation [48].

$$\Lambda_{Th} = X_{(TeO_2)} \cdot \Lambda_{(TeO_2)} + X_{(WO_3)} \cdot \Lambda_{(WO_3)} + X_{(GeO_2)} \cdot \Lambda_{(GeO_2)} \tag{11}$$

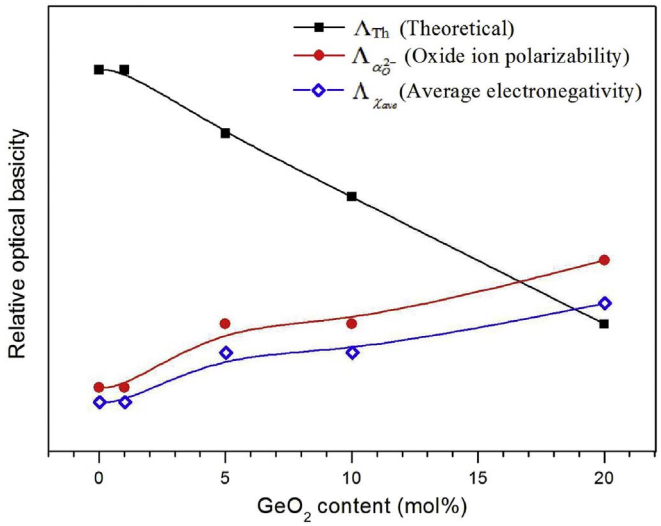

Fig. 10. The variation of optical basicity of TWG*x* glasses as a function of GeO_2 content.

where $\Lambda_{(TeO_2)}$, $\Lambda_{(WO_3)}$ and $\Lambda_{(GeO_2)}$ are the optical basicity values assigned to the constituent oxides and $X_{(TeO_2)}$, $X_{(WO_3)}$ and $X_{(GeO_2)}$ are the equivalent fractions of different oxides, i.e., the contribution of oxide atom to the glass system. The optical basicity values of TeO_2, WO_3 and GeO_2 are 0.96, 1.04 and 0.94, respectively were taken from the literature [42]. The values of Λ_{Th} decrease with increase of GeO_2 content in TWG*x* glasses (see Table 1). R.R. Reddy et al. [43] derived empirical relations to determine the optical basicity in terms of average electronegativity (χ_{ave}) and the oxide ion polarizability ($\alpha_O{}^{2-}$).

$$\Lambda_{\chi_{ave}} = 1.59 - 0.2279\chi_{ave} \tag{12}$$

$$\Lambda_{\alpha_O^{2-}} = 1.67\left[1 - \frac{1}{\alpha_O^{2-}}\right] \tag{13}$$

Though there is a slight difference between the values of $\Lambda_{\chi_{ave}}$ and $\Lambda_{\alpha_o}{}^{2-}$, both show the same increasing tendency with the addition of GeO_2 content (see Table 1). A graphical representation of variation of optical basicity with GeO_2 is shown in Fig. 10. The basicity values obtained from Eq. (12) are slightly smaller and those obtained from Eq. (13) are well matched with the Λ_{Th} values. The optical basicity values of TWG*x* glasses are very close to those reported for 90 TeO_2-10 WO_3 (0.957) [5], (90-*x*) TeO_2-10 GeO_2-*x*WO_3 (0.964–0.982) [19], 70 TeO_2-10 WO_3-20 ZnF_2 (0.882) [36], 90 TeO_2-10 WO_3 (0.973) [43] glasses.

4.8. Refractive index

It is well known that the refractive index (n) of an optical material plays a significant role in designing a new laser or fiber device. There exists number of experimental methods to determine the value of 'n'. In the present investigation, the value of 'n' was determined experimentally using Abbes refractometer with sodium vapour lamp as a light source and they are found decrease with increase of GeO_2 as illustrated in Fig. 1. The value of 'n' can also be determined from the values of optical band gap energy (E_g) using the following formula [42].

$$\left(\frac{n^2-1}{n^2+2}\right) = 1 - \sqrt{\frac{E_g}{20}} \tag{14}$$

The values of refractive index [n(E_g)] obtained from Eq. (14) (see Table 1) are very close to those obtained from the Abbes refractometer. According to Duffy [48], the refractive index of an optical material can also be obtained using the following formula.

$$n = -\log(0.102\,\Delta\chi^*) \tag{15}$$

where $\Delta\chi^*$ is called the optical electronegativity of the medium and it is given as

$$\Delta\chi^* = 0.2688E_g \tag{16}$$

The values of refractive index [n($\Delta\chi^*$)] obtained from Eq. (15) (see Table 1) are slightly deviate slightly from those obtained from Abbes refractometer. The deviation in the measurement of 'n' might be due to the experimental limits. Based on the evaluated thermal, structural and optical properties, it is suggested that the optimum content of GeO_2 to design a novel host material for solid state lasers and fiber devices with negligible non-radiative losses is 10.0 mol%.

5. Conclusions

The tellurite tungstate glasses activated with different contents of GeO_2 were prepared by melt quenching method. Experimentally determined refractive indices are found very close to those obtained from optical band gap (E_g) and optical electronegativity ($\Delta\chi^*$). The TWG*x* glasses show relatively high thermal stability and good glass forming ability. The XRD studies confirm that the studied glasses are highly homogeneous. SEM-EDS results show that the chemical composition of TWG*x* glasses remains unchanged. The IR absorption results show a transformation from TeO_4 units into TeO_3 units. For TWG*x* glasses, the phonon energy is estimated to be 721.34 cm^{-1}. Based on the effect of GeO_2 on various physical, structural and optical properties, it could be concluded that the optimum content of GeO_2 in TWG*x* glasses is 10.0 mol%. Thus, the TWG10 glass has high viability to design a novel host material for solid state lasers and fiber devices.

References

[1] T. Komatsu, Design and control of crystallization in oxide glasses, J. Non-Cryst. Solids 428 (2015) 156–175.
[2] M.S. Al-Assiri, H. Algarni, M. Reben, E. Yousef, H.H. Hegazy, Y.M. AbouDeif, A. Umar, UV–vis-NIR and luminescent characterization of PZCdO: Tm laser oxide glasses, Opt. Mater. 73 (2017) 284–289.
[3] Y. Guo, Y. Tian, L. Zhang, L. Hu, J. Zhang, Erbium doped heavy metal oxide glasses for mid-infrared laser materials, J. Non-Cryst. Solids 377 (2013) 119–123.
[4] D. Li, W. Xu, P. Kuan, W. Li, Z. Lin, X. Wang, L. Zhang, C. Yu, K. Li, L. Hu, Spectroscopic and laser properties of Ho^{3+} doped lanthanum-tungsten-tellurite glass and fiber, Ceram. Int. 42 (2016) 10493–10497.
[5] V. Dimitrov, T. Komatsu, Electronic polarizability, optical basicity and non-linear optical properties of oxide glasses, J. Non-Cryst. Solids 249 (1999) 160–179.
[6] G. Özen, B. Demirata, M.L. Öveçoğlu, A. Genç, Thermal and optical properties of Tm^{3+}-doped tellurite glasses, Spectrochim. Acta A 57 (2001) 273–280.
[7] S. Blanchandin, P. Marchet, P. Thomas, J.C. Champarnaud-Mesjard, B. Frit, A. Chagraoui, New investigations within the TeO_2-WO_3 system: phase equilibrium diagram and glass crystallization, J. Mater. Sci. 34 (1999) 4285–4292.
[8] J.S. Wang, E.M. Vogel, E. Snitzer, Tellurite glass: a new candidate for fiber devices, Opt. Mater. 3 (1994) 187–203.
[9] G.M. Clark, W.P. Doyle, Infra-red spectra of anhydrous molybdates and tungstates, Spectrochim. Acta 22 (1966) 1441–1447.
[10] B.V.R. Chowdari, P. Pramoda Kumari, Structure and ionic conduction in the Ag_2O·WO_3·TeO_2 glass system, J. Mater. Sci. 33 (1998) 3591–3599.
[11] R. Braunstein, I. Lefkowitz, J. Snare, Dipole correlations in TeO_2-WO_3 glass, Solid State Commun. 28 (1978) 843–845.
[12] M.F. Churbanov, A.N. Moiseev, A.V. Chilyasov, V.V. Dorofeev, I.A. Kraev, M.M. Lipatova, T.V. Kotereva, E.M. Dianova, V.G. Plotnichenkoa, E.B. Kryukova, Production of high-purity TeO_2-ZnO and TeO_2-WO_3 glasses with the reduced content of OH^- groups, J. Optoelectron. Adv. Mater. 9 (2007) 3229–3234.
[13] P. Charton, L. Gengembre, P. Armand, TeO_2-WO_3 glasses: infrared, XPS and XANES structural characterizations, J. Solid State Chem. 168 (2002) 175–183.
[14] I. Shaltout, Y. Tang, R. Braunsteint, E.E. Shaishas, FTIR spectra and some optical properties of tungstate-tellurite glasses, J. Phys. Chem. Solids 57 (1996) 1223–1230.
[15] P. Armand, P. Charton, New ternary tellurite glasses: TeO_2-WO_3-Sb_2O_4 and TeO_2-WO_3-Ga_2O_3, Phys. Chem. Glasses 43 (2002) 291–295.
[16] N.V. Ovcharenko, T.V. Smirnova, High refractive index and magneto–optical glasses in the systems TeO_2-WO_3-Bi_2O_3 and TeO_2-WO_3-PbO, J. Non-Cryst. Solids 291 (2001) 121–123.
[17] C.Y. Wang, Z.X. Shen, B.V.R. Chowdari, Raman studies of Ag_2O·WO_3 ternary glasses, J. Raman Spectrosc. 29 (1998) 819–823.
[18] T. Kosuge, Y. Benino, V. Dimitrov, R. Sato, T. Komatsu, Thermal stability and heat capacity changes at the glass transition in K_2O-WO_3-TeO2 glasses, J. Non-Cryst. Solids 242 (1998) 154–164.
[19] G. Upender, C.P. Vardhani, S. Suresh, A.M. Awasthi, V.C. Mouli, Structure, physical and thermal properties of WO_3-GeO_2-TeO_2 glasses, Mater. Chem. Phys. 121 (2010) 335–341.

[20] M.E. Lines, A possible non-halide route to ultralow loss glasses, J. Non-Cryst. Solids 103 (1988) 279–288.
[21] Y. Yang, B. Chen, C. Wang, G. Ren, Q. Meng, X. Zhao, W. Di, X. Wang, J. Sun, L. Cheng, T. Yu, Y. Peng, Spectroscopic properties of Er^{3+}-doped $xGeO_2$-(80-x)TeO_2-10ZnO-10BaO glasses, J. Non-Cryst. Solids 354 (2008) 3747–3751.
[22] G. Monteiro, L.F. Santos, J.C.G. Pereira, R.M. Almeida, Optical and spectroscopic properties of germanotellurite glasses, J. Non-Cryst. Solids 357 (2011) 2695–2701.
[23] S. Rani, S. Sanghi, N. Ahlawat, A. Agarwal, Influence of Bi_2O_3 on thermal, structural and dielectric properties of lithium zinc bismuth borate glasses, J. Alloys Compd. 597 (2014) 110–118.
[24] I. Kashif, A. Ratep, Effect of copper oxide on structure and physical properties of lithium lead borate glasses, Appl. Phys. A Mater. Sci. Process. 20 (2015) 1427–1434.
[25] A. Hruby, Evolution of glass-forming tendency by means of DTA, Czech. J. Phys. B 22 (1972) 1187–1193.
[26] S.S. Babu, K. Jang, E.J. Cho, H. Lee, C.K. Jayasankar, Thermal, structural and optical properties of Eu^{3+}-doped zinc-tellurite glasses, J. Phys. D. Appl. Phys. 40 (2007) 5767–5774.
[27] Y.B. Saddeek, E.R. Shaaban, F.M. Abdel-Rahim, K.H. Mahmoud, Thermal analysis and infrared study of Nb_2O_5-TeO_2 glasses, Philos. Mag. 88 (25) (2008) 3059–3073.
[28] C. Zhao, G.F. Yang, Q.Y. Zhang, Z.H. Jiang, Spectroscopic properties of GeO_2- and Nb_2O_5-modified tellurite glasses doped with Er^{3+}, J. Alloys Compd. 461 (2008) 617–622.
[29] M.M. El-Zaidia, A.A. Ammar, R.A. El-Mallwa, Infrared spectra, electron spin resonance spectra and density of $(TeO_2)_{100-x}$-(WO3)$_x$, and $(TeO)_{100-x}$-$(ZnC1_2)_x$ glasses, Phys. Status Solidi A 91 (1985) 637–642.
[30] Y. Dimitriev, V. Dimitrov, M. Amaudov, IR spectra and structures of tellurite glasses, J. Mater. Sci. 18 (1983) 1353–1358.
[31] A.A. El-Moneim, DTA and IR absorption spectra of vanadium tellurite glasses, Mater. Chem. Phys. 73 (2002) 318–322.
[32] R.A. El-Mallawany, Theoretical and experimental IR spectra of binary rare earth tellurite glasses-1, Infrared Phys. 29 (1989) 781–785.
[33] M.V.V. Kumar, B.C. Jamalaiah, K.R. Gopal, R.R. Reddy, Optical absorption and fluorescence studies of Dy^{3+}-doped lead telluroborate glasses, J. Lumin. 132 (2012) 86–90.
[34] N.F. Mott, E.A. Davis, Electronic Processes in Non-crystalline Materials, second ed., Clarendon Press, New York, 1979, pp. 382–428.
[35] J. Tauc, Optical properties and electronic structure of amorphous Ge and Si, Mater. Res. Bull. 3 (1968) 37–46.
[36] E.S.S. Yousef, Characterization of oxyfluoride tellurite glasses through thermal, optical and ultrasonic measurements, J. Phys. D. Appl. Phys. 38 (2005) 3970–3975.
[37] N. Parveen, V.M. Jali, S.D. Patil, Structure and optical properties of TeO_2-GeO_2 glasses, Int. J. Adv. Sci. Eng. Tech. (Spl. Issue) 3 (2016) 80–85.
[38] R.A.H. El-Mallawany, Tellurite Glasses Hand Book: Physical Properties and Data, 2nd ed., CRC Press, USA, 2016.
[39] F. El-Diasty, F.A.A. Wahab, Optical band gap studies on lithium aluminum silicate glasses doped with Cr^{3+} ions, J. Appl. Phys. 100 (2006) 093511.
[40] F. Urbach, The long-wavelength edge of photographic sensitivity and of the electronic absorption of solids, Phys. Rev. 92 (1953) 1324.
[41] G.A. Evingür, Ö. Pekcan, Optical energy band gap of PAAm-GO composites, Comput. Struct. 183 (2018) 212–215.
[42] V. Dimitrov, S. Sakka, Electronic oxide polarizability and optical basicity of simple oxides. I, J. Appl. Phys. 79 (1996) 1736–1740.
[43] R.R. Reddy, Y.N. Ahammed, P.A. Azeem, K.R. Gopal, T.V.R. Rao, Electronic polarizability and optical basicity properties of oxide glasses through average electronegativity, J. Non-Cryst. Solids 286 (2001) 169–180.
[44] R. Asokamani, R. Manjula, Correlation between electronegativity and superconductivity, Phys. Rev. B 39 (1989) 4217–4221.
[45] E.S. Moustafa, F. Elkhateb, The estimation of the oxide ion polarizability using the B_2O_3-Li_2O_3-Mo glass system, Chem. Mater. Res. 2 (2012) 25–30.
[46] L. Pauling, The Nature of Chemical Bond, 3rd ed., Carnall University Press, New York, 1960.
[47] B.C. Jamalaiah, T. Suhasini, L.R. Moorthy, I.G. Kim, D.S. Yoo, K. Jang, Structural and luminescence properties of Nd^{3+}-doped PbO-B_2O_3-TiO_2-AlF_3 glass for 1.07 μm laser applications, J. Lumin. 132 (2012) 1144–1149.
[48] J.A. Duffy, M.D. Ingram, D. Uhlman, N. Kreidl (Eds.), Optical Properties of Glasses, Am. Ceram. Soc., Westerville, 1991.